A&A manuscript no.
(will be inserted by hand later)

Your thesaurus codes are:
06 (06.03.2, 06.24.1)

ASTRONOMY AND ASTROPHYSICS
June 30, 1998

Analysis and comparison of loop structures imaged with NIXT and Yohkoh/SXT

V. Di Matteo[1], F. Reale[2], G. Peres[2], and L. Golub[3]

[1] Osservatorio Astronomico, Piazza del Parlamento 1, 90134 Palermo, Italy (e-mail: dimatteo@oapa.astropa.unipa.it)
[2] Dipartimento di Scienze Fisiche e Astronomiche, Università di Palermo, Sezione di Astronomia, Piazza del Parlamento 1, I-90134 Palermo, Italy, e-mail: reale@oapa.astropa.unipa.it, peres@oapa.astropa.unipa.it
[3] Smithsonian Astrophysical Observatory, 60 Garden Street, Cambridge, MA 02138, USA, e-mail: golub@corona.harvard.edu

Received .... / Accepted ....

Abstract. We analyze and compare five coronal regions simultaneously observed by NIXT and Yohkoh/SXT on April 12, 1993. The compact loop structures (length $\sim 10^9$ cm) imaged in three regions with NIXT and with SXT have a good general morphological correspondence. A large scale ($\approx 1.7 \times 10^{10}$ cm) and an intermediate scale ($\approx 5 \times 10^9$ cm) structure observed in the NIXT image have no obvious counterpart in the SXT image. The pressure of the loop plasma detected by NIXT is derived from the brightness profile along the loops by applying a method based on loop models. The pressure of the loop plasma in the SXT band has also been derived from loop models on the basis of the temperature obtained from the standard Yohkoh data analysis. NIXT pressures are systematically lower than those found with SXT. By comparing the measured total loop luminosity to that expected on the basis of loop models, we constrain quantitatively the volume filling factor of the plasma emitting respectively in the NIXT and SXT bands. The filling factors obtained in the NIXT band for the compact and intermediate loops are very low ($10^{-3} - 10^{-2}$), but they are of the order of unity for the large structure. The low filling factors suggest a strong loop filamentation. The filling factors for the compact structures are instead of the order of unity in the SXT band. We discuss our results and propose a scenario for their interpretation.

Key words: Sun: corona – Sun: X-rays

1. Introduction

Achieving high temporal and spatial resolution in solar X-ray observations is one of the main challenges of solar coronal physics. There is evidence that the solar corona is structured down to sub-arcsec dimensions (Gomez et al. 1993). On the other hand, plasma theory applied to the corona suggests that the magnetized plasma is subject of significant filamentation (van den Oord 1992, Litwin & Rosner 1993, Velli 1995) Such a filamentation has also been invoked as a means to generate and distribute efficiently heat released by instabilities in magnetized plasma (Parker 1988).

The SAO Normal Incidence X-ray Telescope (NIXT, Golub & Herant 1989) represents one of the fundamental steps toward obtaining the sub-arcsec spatial resolution required to observe the very small scales. For an exhaustive analysis and interpretation of the observations made by the NIXT it is important to obtain information about the physical conditions of the emitting plasma. Such a task is not straightforward with NIXT, since its single and narrow spectral band practically inhibits the application of temperature diagnostic methods, and in particular the filter ratio method used by wide band telescopes such as the Soft X-ray Telescope (SXT) on board the Yohkoh satellite.

This work is devoted to analyze and interpret the observation of selected coronal loop structures made simultaneously by NIXT and Yohkoh/SXT on April 12, 1993 (see also Yoshida et al. 1995), in order to obtain a detailed and accurate scenario taking advantage of the different insight provided by the two instruments.

Our analysis is enriched by the determination of the pressure of the plasma emitting in the NIXT band, made possible by the application of a method developed previously by Peres et al. (1994, hereafter Paper I). This method is based on extensive loop modeling and allows us to evaluate the plasma pressure directly from the analysis of the NIXT brightness distribution along the loops.

Our models show that the pressure, in a hydrostatic loop of given length, determines the temperature distribution along the loop of the confined plasma. If the plasma is observed through a narrow spectral band, such as the NIXT band, including very few spectral lines with specific formation temperatures, the brightness distribution along the loop will be strongly influenced by the plasma temperature.

Send offprint requests to: F. Reale

On the basis of the loop emission in the NIXT passband, synthesized from the results of hydrostatic loop models, it has been shown in Paper I that the shape of the brightness distribution changes with pressure, yielding bright footpoints in high pressure loops and a more uniform brightness in lower pressure loops. Here we present the first quantitative application of this pressure diagnostics, which can be applied, after proper calibration, to any imaging instrument with a narrow pass-band around 10^6 K.

As an implication of the pressure determination, by comparing the observed NIXT loop total luminosity to that predicted from hydrostatic models, we are able to estimate the volume filling factor of the plasma emitting in the NIXT band and the level of filamentation in the observed loops.

In order to obtain a scenario as complete as possible we perform the same kind of analysis on Yohkoh/SXT data, for which direct temperature diagnostics are possible and thereby obtain information complementary to that of NIXT.

NIXT and Yohkoh/SXT are characterized by different optics and detectors, which result in significant differences in their response to the plasma temperature. NIXT is based on multi-layer normal-incidence mirrors which yield high reflectivity and a high spatial resolution (1.2") in a narrow spectral band centered on 63.5 Å and 1.4 Å wide (Golub et al. 1990). This band contains the intense MgX at 63.5 Å and Fe XVI at 63.7 Å lines, which determine a maximum instrument sensitivity to plasma radiating between 1 and 3 MK. Yohkoh/SXT (Tsuneta et al. 1991) instead is based on grazing-incidence optics, has a lower spatial resolution (2.5"), a much wider spectral band, with the possibility of using various filters, and is more sensitive to higher temperatures (roughly speaking above 2.5 MK).

Given the sensitivity to plasma at different temperatures, we expect *a priori* significant differences in the detectable plasma and therefore both in the morphological appearance of the coronal structure and in the physical conditions of the detected plasma. Indeed, the sensitivity to different temperatures has been invoked by Yoshida et al. (1995) to explain the significantly different appearance of some coronal structures, different from those selected by us, detected in the two simultaneous observations made on April 12, 1993.

Our analysis of the two observations, and their combination and comparison, allow us to go beyond the simple confirmation that the two instruments look at plasmas in different thermal conditions, and provide us with a very rich scenario of the loop structuring and conditions, as we will illustrate in the following.

In section 2, we select and describe the loop structures as observed with NIXT and Yohkoh; in section 3 we analyze the NIXT data, and evaluate the plasma pressure and the volume filling factor; in section 4 we analyze the corresponding structures in SXT images. In section 5 we discuss the results and draw our conclusions.

2. The Loop Structures

Fig. 1 and 2 show the full-sun NIXT and SXT images, respectively, taken virtually simultaneously on April 12, 1993. The NIXT data were taken between 17:17 and 17:23 UT, the SXT data between 17:11 and 17:28 UT. The NIXT image is made of 2000×2000 pixels of 1.2"×1.2", the SXT image of 512×512 pixels of 4.91"×4.91". The SXT image results from a combination of two single exposures of 78 and 2668 ms in the Al.1 filter (Tsuneta et al. 1991, see Sect. 4 for more details). The images have been aligned by using a fitting procedure applied to the disk limbs.

As described by Yoshida et al. (1995), many loop structures are clearly visible in the SXT image, both inside and outside the large active regions close to the disk center. There are two other active regions, one on the south-west and the other, very large, on the east limb of the disk. The loop structures are less evident in the NIXT image, although some of them are clearly visible inside and close to the active region at the center of the disk.

The loops to which we apply our pressure diagnostics have been selected from the NIXT full disk image (Fig. 1). The identification of loop structures from X-ray images is, in general, non-trivial; since the Skylab era (e.g. Vaiana 1976) it has become clear the need to identify loops with the aid of magnetograms. Therefore we have taken advantage of magnetograms to identify the loop footpoints. The magnetograms were taken by P. Hartmann of Kitt Peak Solar Observatory between 15:11 and 16:06 UT, about one hour before the X-ray images. We have corrected for the shift due to solar rotation and aligned the magnetograms to the images. We have then selected rectangular regions including single loop structures with the following two basic requirements:

1. the candidate loop structures in the NIXT image have to be isolated from other structures;
2. the extremes of the loop structures in the X-ray image must correspond to opposite polarity spots in the magnetograms.

The need for an unequivocal identification of the loop structures may impose a bias to select bright, and therefore preferentially high pressure, loops but we will show that our small sample includes pressure values spanning more than a decade, from values typical of quiet regions to those of active regions. We have selected five regions, which we will identify in the following with **A**, **B**, **C**, **D**, **E** in decreasing order of solar latitude, as shown Fig. 1 and, in more detail, in Fig. 3. Their characteristics, as derived from the analysis of the NIXT image, are reported in Table 1, together with relevant physical parameters derived according to the procedures illustrated in Sect.3.

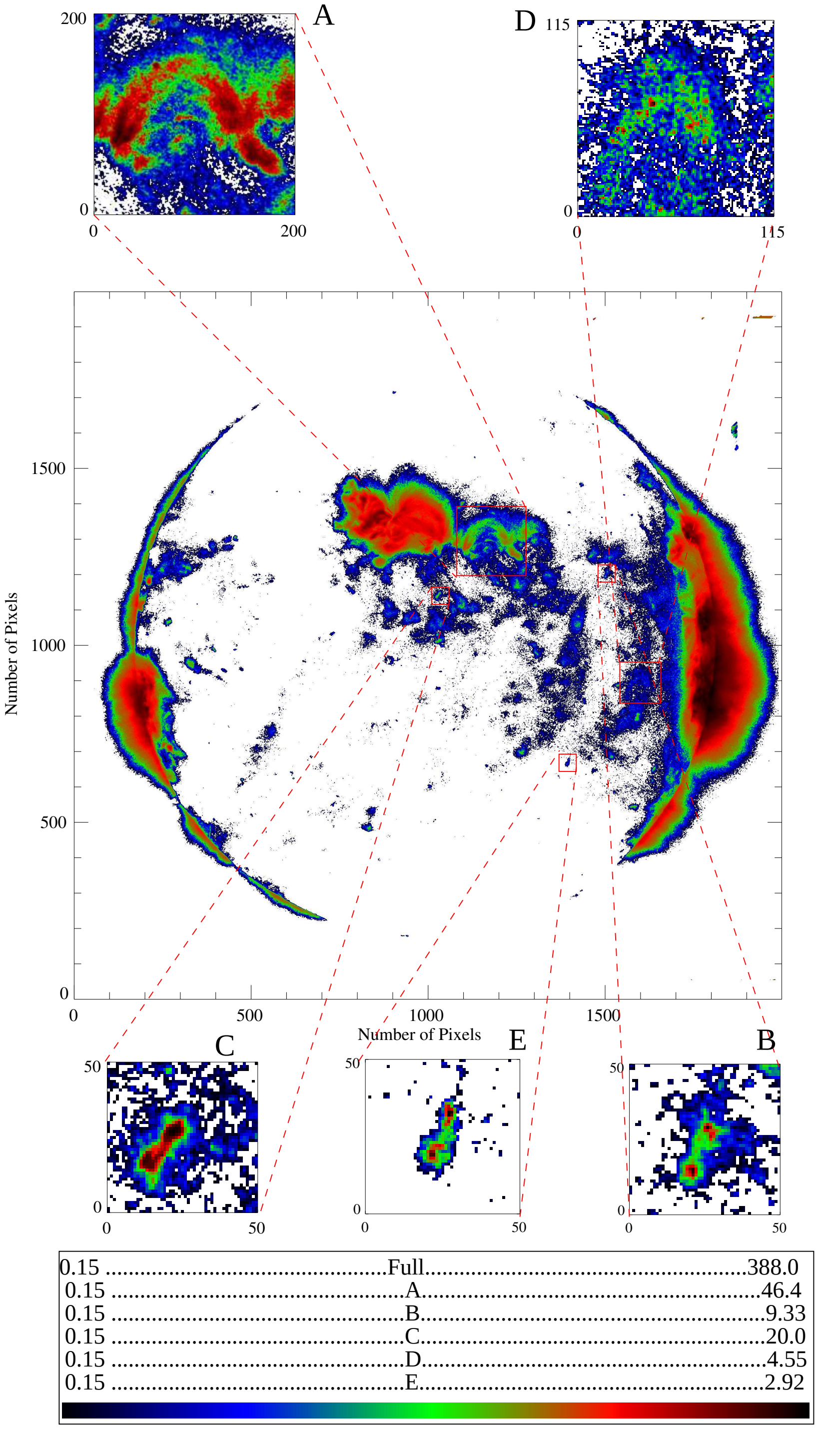

Fig. 1. NIXT solar image of April 12, 1993: the insets expand the regions where loop structures have been selected for analysis. The brightness color scales, indicated at the bottom for all panels (full disk and subregions), are logarithmic (cgs units).

Region **A**, slightly to the east of the central active region (Fig. 1), shows a large loop structure (the distance between the footpoints is $\approx 10^{10}$ cm) with evident footpoints, which correspond to regions of opposite polarity in magnetograms. The loop appears to lie in a plane almost perpendicular to the line of sight, and it does not overlap with other structures, in spite of its large extension, except for a bright structure not far from the apex.

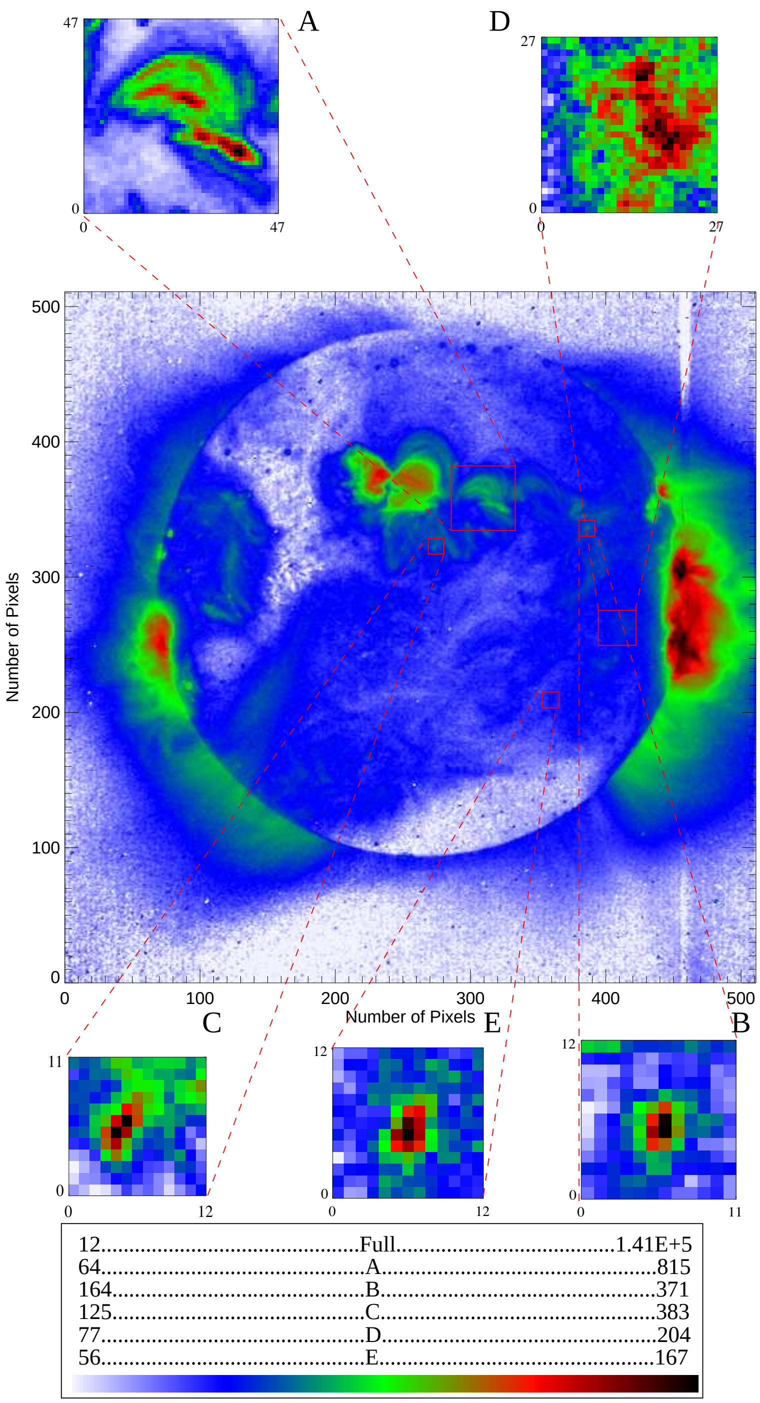

Fig. 2. Yohkoh/SXT solar image of April 12, 1993: the insets expand the same regions as the corresponding insets in Fig.1. As in Fig.1, the color scales are logarithmic (DN/s).

Regions **B**, **C** and **E** contain candidate isolated loops of relatively small extension ($\approx 10^9$ cm). The loops connect opposite polarities, thus suggesting that they are seen from above.

The loop structure in region **D** is very faint and not well defined. The results concerning this region will therefore be taken with proper care. Along this arch there are some small bright structures, which mix significantly with the loop.

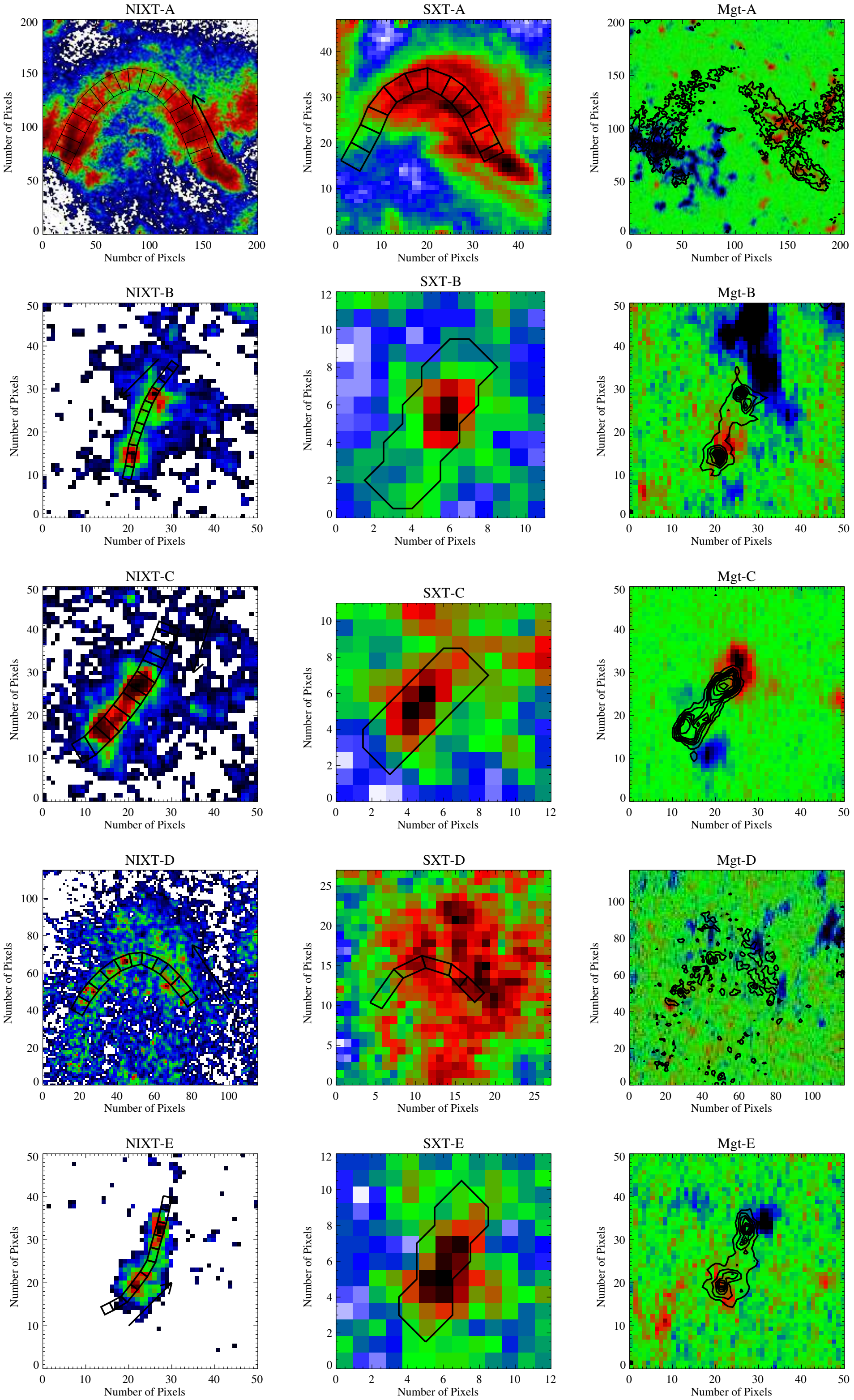

Fig. 3. Analyzed loop structures: the first and second columns show the insets of Figs. 1 (NIXT image) and 2 (SXT image) respectively, the third column the corresponding magnetograms (courtesy of NSO/Kitt Peak, from a collaboration of NSF/NOAO, NASA/GSFC and NOAA/SEL). In the NIXT frames the solid strips bound the inferred isolated loops, divided into rectangular sectors for the analysis. The corresponding strips and the appropriate division into sectors are marked also in the SXT insets. In the NIXT frames, the arrows indicate the positive direction of the NIXT brightness profiles in Fig. 5. Contour plots of NIXT brightness are shown in the magnetograms. The color scales of the magnetograms are linear (blue negative, green neutral, red positive) and range between -146 G and 146 G for regions A and C and between -73 G and 73 G for regions B, D, and E.

Table 1. Analysis of loop structures imaged with NIXT.

	A	B	C	D	E
Area	241.2" x 241.2"	61.2" x 61.2"	61.2" x 61.2"	139.2" x 139.2"	61.2" x 61.2"
latitude[a]	22.44°	13.98°	9.70°	−7.64°	−24.20°
longitude[a]	12.22°	37.32°	2.96°	47.47°	26.59°
$\mathcal{D}^b$ (10^9cm)	10.2 ± 0.6	1.32 ± 0.06	1.22 ± 0.15	3.41 ± 0.21	1.25 ± 0.06
L^c (10^9cm)	8.5 ± 0.5	1.31 ± 0.06	1.01 ± 0.13	2.71 ± 0.17	0.99 ± 0.05
x^d (pixel)	20	2	5	7	2
y^d (pixel)	10	3	3	6	3
N^d (pixel)	13	5	3	9	3
$\mathcal{C}^e$	9.5 ± 1.2	2.2 ± 0.2	3.0 ± 0.6	2.23 ± 0.09	2.9 ± 0.2
p^f (dyne/cm^2)	$0.081^{+0.002}_{-0.007}$	$0.52^{+0.05}_{-0.03}$	$0.33^{+0.02}_{-0.03}$	$0.23^{+0.02}_{-0.01}$	$0.53^{+0.03}_{-0.07}$
$Log(T_M)^f$ (°K)	6.11	6.09	5.98	6.08	6.06
$Log(ff)^f$	-0.64 ± 0.15	-2.63 ± 0.11	-2.14 ± 0.13	-2.70 ± 0.12	-2.99 ± 0.13

[a] - Coordinates of the center of the selected regions;
[b] - Distance of the footpoints;
[c] - Loop half-length;
[d] - Width, length and total number, respectively, of the sectors in which each loop has been divided for the analysis;
[e] - Average luminosity contrast between the sectors at the footpoints and the apex of the loops;
[f] - pressure, maximum temperature (obtained from scaling laws) and volume filling factor, respectively, of the loop plasma emitting in the NIXT band.

3. The Analysis of NIXT data

3.1. The method

The approach to deriving the physical conditions inside the loops seen by NIXT, in a single narrow spectral band, is to compare the brightness distribution along the observed loop structures to that resulting from hydrostatic loop models. The SXT observations confirm that the emitting structures do not change significantly during the observation over a time scale of $\sim$ 15 minutes, according to the general evidence that such structures live over time scales longer than the radiative and conductive cooling times (hours).

Therefore, in agreement with the hypothesis of Paper I, we consider a hydrostatic model of a coronal loop, semicircular, of constant cross section, symmetric with respect to its apex; the equations are those of plasma hydrostatic equilibrium and of energy balance among radiative losses, thermal conduction and a phenomenological term of local heat input in the plasma. The lower boundary of the loop is set at 2 10^4 K. We refer to Paper I for further details.

The models are uniquely identified by p_0, the plasma pressure at the base of the arch and by L the loop semilength, which determine T_{max}, the maximum plasma temperature, located at the loop apex; these parameters are linked by the scaling laws of Serio et al. (1981).

Paper I shows that the brightness distribution along the loops, as observed by NIXT, depends on the loop base pressure. For high base pressure ($p \gtrsim 1$ dyne cm^{-2}, for loops with $L \sim 10^9$ cm) the loop brightness is high and has a sharp maximum at the loop base, whereas the brightness is much more uniform (and lower) at lower pressure. The dependence of the emission distribution on pressure is a consequence of the dependence of the maximum temperature on pressure, according to the Serio et al. (1981) scaling law. This dependence of emission profile on plasma pressure occurs for any loop length considered, although the specific maximum temperature and brightness distribution depend also on the loop length.

On the basis of these results, in Paper I it is expected that footpoints are very bright immediately above the transition region in all the high pressure loops, typically found in active regions, and therefore it is possible to identify high pressure coronal regions in NIXT pictures. On the other hand, faint loop structures, if detected at all, are expected to be observed as entire loops in NIXT images, given the uniform brightness distribution predicted by the modeling.

Given the property that the profile of the brightness along the loop depends mostly on the plasma pressure, the loop plasma pressure can be determined by matching the NIXT brightness distribution, synthesized from the loop models, to the observed one. However obtaining a brightness distribution directly comparable with models is, in practice, very difficult, because the loop orientation is unknown. Furthermore the brightness profiles derived along the loops typically show fluctuations which make an accurate comparison even more difficult.

Therefore we have chosen to take the brightness contrast ($\mathcal{C} = b_{foot}/b_{top}$) of the footpoints to the apex of the loop as indicator of the brightness distribution shape. Operatively the loops that we analyze are those for which we are able to mark an arc between two footpoints, and this is possible only as long as the footpoints are brighter than the rest of the loops. This implies that our selected loops will all have $\mathcal{C} \gtrsim 1$, i.e. they are relatively high pressure loops. Of course, this implies a selection effect, but it is unavoidable also because low pressure loops are faint.

Even the contrast $\mathcal{C}$ depends moderately on the loop orientation with respect to the observer, as shown in Fig. 4, which reports the contrast $\mathcal{C}$ between the luminosity in the NIXT band at the base and at the apex of model loops of various lengths vs. the base pressure. The luminosity is obtained by integrating the emission per unit volume on the labeled bin size (in pixels) along the loop. Each column shows the resulting contrast for a different extreme orientation: side view and top view, respectively. The contrasts are higher for loops seen from the top, as may be expected since the footpoint luminosity includes a significant vertical section of the loop.

For a given semilength and for low contrasts, $\mathcal{C}$ generally increases with the pressure as expected. However, above a contrast threshold, which depends on the spatial integration step, on the loop orientation and on the loop length, the contrast has a maximum and then decreases. For such high contrasts therefore we do not have a univocal pressure diagnostics. This limit does not affect our results: as we will see in the following, we have been able to find univocal pressure values for all our selected loops. Since all selected loops are well inside the solar disk we have neglected the effect of different orientations with respect to the loop axis.

The loop models yield results per unit cross sectional area. The expected total loop luminosity is then obtained by multiplying the model brightness integrated along the loop by the loop cross-sectional area. This luminosity can be compared to the luminosity measured on the calibrated images. The ratio of the two provides a quantitative measurement of the volume fraction effectively occupied by the emitting plasma, i.e. the loop plasma filling factor in the instrument band. This ratio is expected to be always smaller than (or at most equal to) unity, i.e. the model luminosity should always be larger than (or equal to) the measured luminosity. Errors in the aspect determination and on the loop cross section however allow for ratios larger than 1.

3.2. The results

3.2.1. The pressure

In order to apply the pressure diagnostics we first evaluate the half-length L of the selected loops. Assuming semicircular loops (such an assumption is not critical), the half-length can be obtained from the distance between the footpoints d, $L = \pi d/4$. For d we have taken the linear distance between the brightest pixels at the two opposite sides of a loop. This was not possible for region **D**, for which, instead, we have taken the distance between the magnetic poles from the magnetograms. The main error source on d is associated with the transversal section of the loop, as determined from the analysis of the brightness distribution perpendicular to the magnetic field lines, taken close to the loop footpoints, where the signal is more intense. The position of the loop footpoints is generally included within the transversal profiles and to be conservative we have taken half of the full width half maximum (FWHM/2) of one of the two profiles (the more well-behaved) as the inaccuracy on the position of the footpoint. The error on d then will be the root sum square of the uncertainties of the two footpoint positions, i.e. FWHM/$\sqrt{2}$. The values obtained for L are shown in Table 1, and are all between 10^9 and 10^{10} cm.

Then we extract the brightness distributions along each loop. We first mark a sequence of pixels which follow the loop structure as close as possible. The pixels are then connected by a line. In order to increase the signal to noise ratio, we consider a strip of pixels centered on this path, and divide this strip into sectors with approximately the same area (i.e. including the same number of pixels). The FWHM of the transveral brightness distribution described above is taken as the strip width x. As size of each sector along the loop we take the characteristic length in which the brightness decreases from the maximum to 1/3 of the maximum, and in such a way that: i) the number of sectors is odd, so that the central sector, usually the one containing the brightness minimum, is univocally and well identified; ii) the number of sectors is ≥ 5, enough to obtain a proper brightness distribution. For region **D**, the low signal required to select sectors as large as possible: ~ 50 pixels are contained in each of the 11 sectors selected. This selection allows us also to obtain a well-defined brightness profile, as well as to avoid that the bright points are included in the region of minimum intensity.

The pixel brightness has then been averaged on each sector and the resulting brightness distributions along the paths are shown in Fig.5.

As described in Section 3.1, the brightness contrast between the footpoints and the apex is the figure used to evaluate the pressure in the selected loops. Before computing this contrast, the background brightness is subtracted from the brightness along the loops. The background brightness for each loop has been evaluated in a small region outside of the loop, close to the loop apex, the point of minimum brightness. Its value changes from region to region, and ranges from 10% to 40% of the brightness at the loop apex. For each loop we obtain two values of the contrast, one for each footpoint ($\mathcal{C}_1$ and $\mathcal{C}_2$), which in general differ from each other. We have then taken the average $\mathcal{C} = (\mathcal{C}_1 + \mathcal{C}_2)/2$ as the best contrast estimate and $\Delta\mathcal{C} = |\mathcal{C}_1 - \mathcal{C}_2|$ as its uncertainty. We have estimated this uncertainty to be dominant with respect to others, such as fluctuations, statistical noise, and it includes that due to the chance alignment of other structures. We have verified on strips wider than 2 pixels, that halving the strip width changes the contrast values by less than 10%.

From the loop half-length L and the brightness contrast $\mathcal{C}$, the pressure is evaluated with the method outlined in Sect.3.1. In order to compare homogeneous quantities,

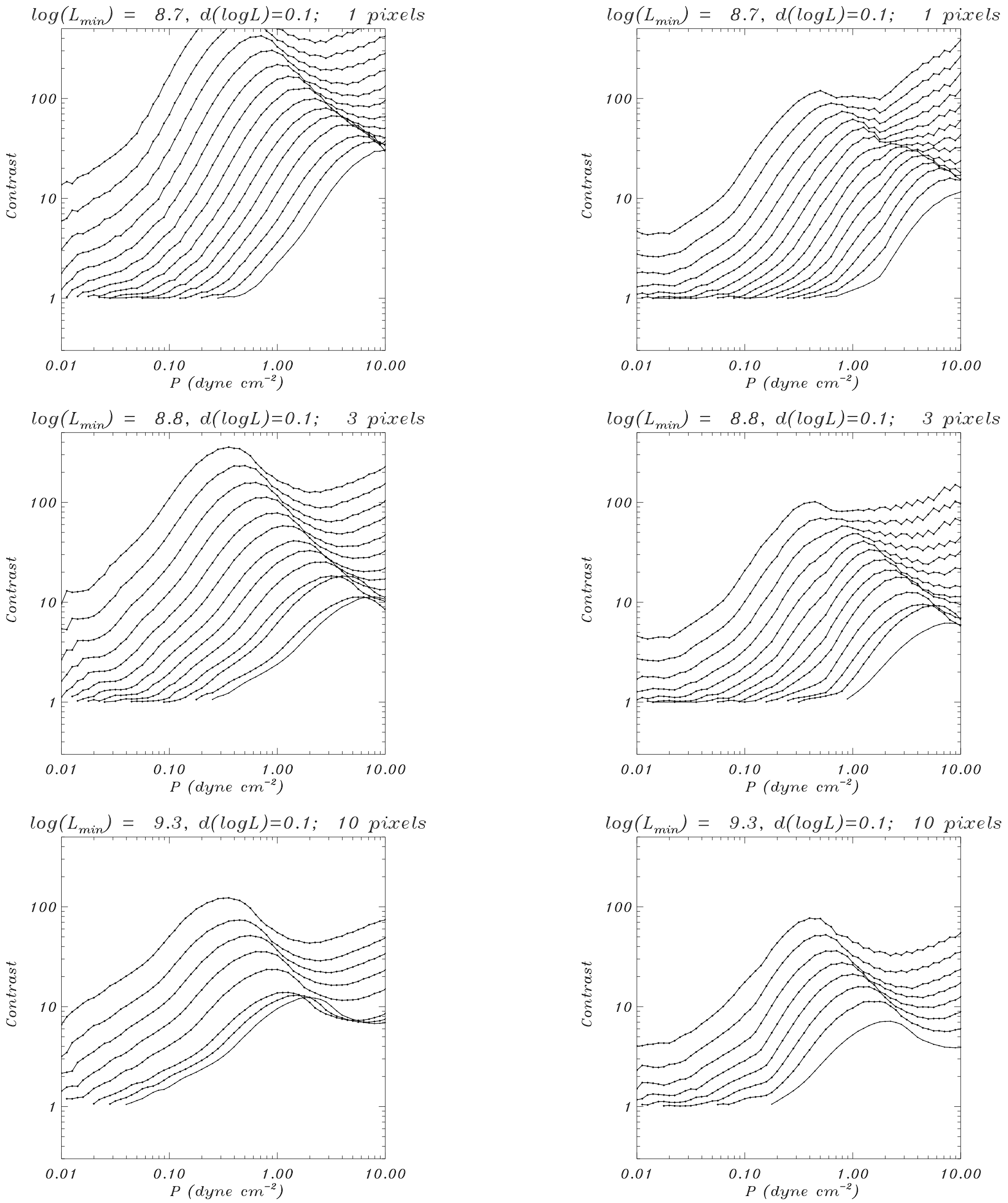

Fig. 4. Luminosity contrast of loop footpoint with respect to the loop apex in the NIXT band vs pressure, as predicted from loop model. Each solid line pertains to model loops with the same length. The lowest line is for the shortest loop (L_{min}), higher lines are for longer and longer loops with the labeled step of increasing length. The three rows of figures are for different sizes (in pixels, in the figure labels) of the length step along the loop over which the luminosity is integrated. In the first column the contrast is computed assuming the loop as seen from above, the second as seen with a front view.

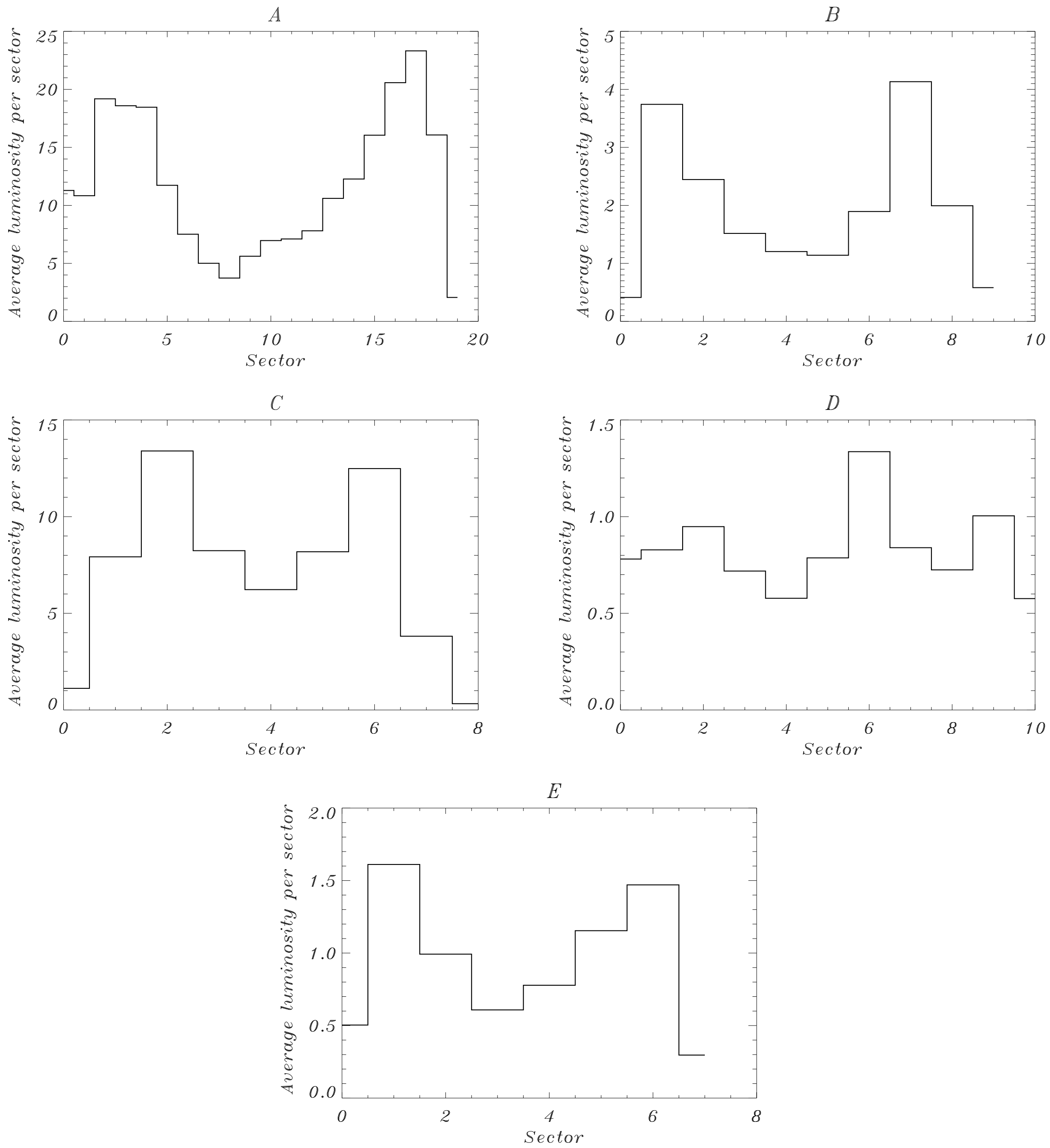

Fig. 5. Loop brightness profiles along the paths drawn in Fig.3. The brightness is averaged in the sectors marked in Fig.3.

we bin the plasma emission synthesized in the NIXT band from the models along the loop, with bin sizes of the same length as that of the loop sectors selected on the NIXT image, i.e the number of pixels y in Table 1. The resulting contrasts are shown in Table 1.

Data and models can now be compared on homogeneous ground. For a detailed comparison, we have generated a grid of loop models as fine as to minimize the uncertainty due to the discreteness of the grid. For each estimated loop length, the base pressure of the model loops range between 0.1 and 10 dyne/cm^2, increasing with logarithmic step $\Delta \log p = 0.5$. The jump of pressure from one model to the next is $\sim 2\%$ whereas the average uncertainty from the data is $> 5\%$. From all the models we derive the brightness contrast between the base and the top sector, considering the two possible extreme loop orientations with respect to the observer, as seen from the front and from above (see Sect. 3.1). The loop morphology is taken as good evidence that loops in regions **A** and **D** are seen from the front, and therefore their contrast can be compared to the contrasts in the first column of Fig. 4, and that the others are seen from above (second column in Fig. 4).

The best value of the pressure of the observed loop with contrast $\mathcal{C} \pm \Delta\mathcal{C}$ is the pressure of the model whose contrast is the closest to $\mathcal{C}$. The uncertainty on the pressure is determined from $\Delta\mathcal{C}$ in the same way. The pressure values p are shown in Table 1, together with the loop maximum temperature T_M estimated from the scaling laws of Serio et al. (1981).

We have verified that the other loop orientation reduces the pressure by a factor ~ 4 for loops **A** and **D**, and increases it by a factor ~ 2 for the others. The values of the NIXT filling factor, discussed in the following, are instead much less affected by this assumption, except for that of loop **A**, which becomes larger than unity if the loop is assumed to be seen from above, clearly an unreasonable result.

In the following we summarize and discuss the results for each selected loop:

Loop A : The resulting relatively low pressure value is consistent with the loop being a large scale structure, with a diameter $\approx 15\%$ of the solar radius. The temperature estimated from scaling laws is close to that to which NIXT is most sensitive.

Loops B, C, E : due to their similarity, these compact structures can be discussed together. Their dimensions are typical of active region loops, but the pressure values are somewhat lower. Also their temperature is in the range of the instrument maximum sensitivity.

Loop D : This loop of intermediate size has an intermediate pressure value, and yields a temperature similar to the others.

In general we notice that the smallest selected loops tend to yield higher pressures than the largest ones. We cannot exclude a selection effect of the instrument passband, which tends to detect more easily structures with plasma at temperatures close to the temperature of maximum sensitivity. From the point of view of the scaling laws this is equivalent to fixing the product $p\ L$, so that smaller L implies larger p.

3.2.2. The volume filling factor

The length L and the pressure p uniquely identify a loop model among those of Serio et al. (1981), of which we have synthesized the emission in the NIXT band. We now compare the total observed loop luminosity to that expected from the models. For a homogeneous comparison with the image calibrated brightness, we integrate the emission per unit volume derived from the model on the sector length y, multiplied by the width x, and divided by the same sector section z as the one used for the data. We find that the model brightness is sistematically larger than the measured one, consistent with the expectation of plasma volume filling factors generally smaller than 100%. The ratio of the measured and expected brightnesses provides us with a quantitative estimate of the volume filling factor for loops visible in the NIXT band, shown in the last row of Table 1. The uncertainties take into account also an average data calibration error of 20%. The results are:

Loop A : the filling factor is relatively high, comparable to unity.

Loops B, C, D, E : the filling factor is very small, between 0.1% and 1%.

Such a wide range of filling factor values, spanning three orders of magnitude, excludes the presence of dominant calibration systematic effects on the results.

4. The Yohkoh/SXT data: morphology, pressure and filling factor

Two SXT images, close in time and made in two different filters, allow us to obtain maps of temperature and emission measure. The temperature is obtained directly from the ratio of the brightness in the two different filters. The emission measure is obtained from the ratio:

$$EM = \frac{B_k}{G_k(T)} \tag{1}$$

where B_k and G_k are the pixel luminosity and the expected luminosity per unit emission measure in the k-th filter.

The SXT data are taken in the Al.1 and AlMg filters (Tsuneta et al. 1991). We have combined couples of short and long exposure images (78 and 2668 ms in the Al.1 filter, 168 and 5338 ms in the AlMg filters) to obtain a higher dynamic range. In order to identify the same regions already selected in the NIXT image, the SXT and NIXT images have been co-aligned in the same way as we did with the magnetograms. In Figs.2 and 3 we show these regions as observed with the SXT. Region **A** contains a larger and more complex structure than that detected by NIXT, presumably a bundle of adjacent loops, whereas NIXT seems to detect a single structure. The same path as marked on the NIXT image does not seem to mark so clearly a single loop as, instead, it does on the NIXT image. Regions **B**, **C**, and **E** are characterized by smaller bright structures, whose size is of the order of one pixel. Region **D** does not show any clearly identifiable structure on the SXT images.

The same five paths as in the NIXT image have been marked on the SXT images. We have applied our analysis on all five regions, even if for regions **A** and **D** there is no clear correspondence with loop-like structures. We have then considered strips with the same width as for NIXT images. This has been possible only for regions **A** and **D**, because the SXT pixel is 4 times larger than the NIXT pixel; for the other smaller loops we have considered a minimal strip width of 2 pixels. The strips of loops **A** and **D** has also been divided into sectors, so as to have an idea of the temperature and emission measure distribution within the loop. A single sector has been instead considered for the other loops. The detected emission has been integrated in each sector.

The resulting temperature and emission measure distributions for regions **A** and **D** are practically uniform along the selected paths within the uncertainties. On the other hand, since the paths traced to follow isolated loops on the NIXT image do not mark clearly loop structures on the SXT images, we do not expect to obtain any well-defined trend, comparable to those typical from loop models.

In order to evaluate the loop pressure from the SXT data, we assume the temperature averaged on the marked strips, T_{eff} as the loop average temperature (of the plasma emitting in the SXT band). We then consider the same grid of model loops as those used for the NIXT analysis (Sect.3) and compute their average temperature T_{mod} from the ratio of the total loop emissions synthesized in the two selected SXT filters.

Then we take as loop pressure is the base pressure of the loop model which yields $T_{mod} \approx T_{eff}$. From the ratio of the total detected loop emission to the total model emission (in one filter) multiplied by a cross-section diameter, we then derive the volume filling factor of the plasma emitting in the SXT band. The cross-section diameter has been determined as equal to the SXT FWHM at one of the footpoints, as done in the analysis of NIXT data, for the loops well-defined in SXT (**B**, **C**, **E**), and directly as equal to diameter as determined in the NIXT analysis for loops **A** and **D**. It is worth noting that the average temperature considered here is not the same as the temperature at the loop apex, the same used in the scaling laws for hydrostatic loops, but instead it is systematically lower, being an average including plasma at lower temperatures.

Table 2 shows the temperature, the emission measure per pixel, the cross-section diameter (in pixels), the loop pressure and the filling factor as derived from the method above.

As is clear from Table 2, all the pressure values derived from SXT are systematically higher (a factor 3 to 9) than those derived from NIXT. This is essentially due to the different passbands of the two instruments which select plasma at different temperatures (and therefore pressure). Even for the large region **A** the pressure value is more similar to those of active region loops. As occurred for NIXT, the compact loops have higher pressure, typical of core active regions. The filling factors are all considerably higher that those obtained from NIXT. The values for the compact structures **B**, **C**, **E** are comprised in the range 0.1–1. Such values, not far from unity, indicate loops filled up with plasma emitting in the SXT band. Indeed, the real filling factor may be closer to unity than the obtained one, because the relatively limited resolution of the SXT image forces us probably, especially for small loops, to consider volumes outside the loop.

The value for region **D** is compatible with unity. Since this structure is not well-defined in the SXT image, we will not discuss it any further. Instead the very high value obtained for region **A** deserves some comments. As discussed previously, the boundaries which clearly identify a single loop structure on the NIXT image do not identify it as clearly on the SXT image. In the SXT image the region appears relatively less bright than the immediately surrounding region. At a first glance, one may think that the different pass-bands make the loop footpoints appear brighter in the NIXT band and the apex in the SXT band. If this were the case, we would still have obtained a realistic value of the filling factor. Such a high value instead indicates that *SXT is detecting a structure or structures different and distinct from that visible in the NIXT image and falling in the same field of view.* In fact, it is possible to obtain filling factor values comparable to, or smaller than, unity only if we consider a loop or bundle of loops considerably smaller/shorter than that identified in the NIXT image (as shown in Fig.2). These loops therefore are not the same loops as the NIXT loop.

An alternative way to evaluate the loop plasma pressure is to derive the density from the emission measure as in Eq. (1), by making an assumption on the emitting volume V:

$$n = \sqrt{EM/V} \qquad p = 2k_B nT \tag{2}$$

where fully ionized gas has been assumed.

We can estimate the relevant volume by considering the loops as enclosed in the areas marked in Fig.3. We can then evaluate the cross-sectional area for two extreme values of loop depth along the line of sight: a) the unit depth (1 pixel = 4.9"), which corresponds to a minimal volume and therefore will yield an upper limit on pressure; b) the depth for a toroidal loop, with circular cross section with diameter equal to the strip width; in this case the "effective" depth, i.e. taking into account that it varies across the loop, is $\sqrt{\pi/4}$ of the cross diameter, and it should yield a maximum volume and therefore a lower limit on pressure.

We have verified that the pressure values derived from the EM with the above assumptions on the volume invariably lead to unreasonably high SXT filling factors i.e. much larger than one, for all our selected loops. Indeed this approach is not self-consistent since the assumptions on volume do not take into account the loop filamentation.

Table 2. Loops as imaged by Yohkoh/SXT

	$\mathrm{Log}_{10}(\mathrm{T}^{a}_{eff})$ K	$\mathrm{Log}_{10}(\mathrm{EM}^{b}_{pixel})$ cm^{-3}	d[c]	p[d] dyne/cm^2	ff[e]
A[f]	6.243 ± 0.005	44.69 ± 0.02	5	$0.39^{+0.05}_{-0.04}$	$(7.8^{+3.5}_{-2.4})^{g}$
B	6.28 ± 0.05	44.3 ± 0.3	2	$3.5^{+2.1}_{-1.3}$	$0.1^{+0.3}_{-0.08}$
C	6.24 ± 0.03	44.5 ± 0.2	2	$2.8^{+1.2}_{-0.8}$	$0.4^{+0.6}_{-0.2}$
D[f]	6.19 ± 0.02	44.48 ± 0.07	3	$0.6^{+0.2}_{-1.3}$	$(1.4^{+1.3}_{-0.7})^{g}$
E	6.18 ± 0.06	44.4 ± 0.2	3	$1.6^{+1.2}_{-0.7}$	$0.3^{+1.1}_{-0.3}$

[a] - Loop average temperature
[b] - Average emission measure per pixel
[c] - Loop cross-section diameter (in pixels)
[d] - Pressure obtained from SXT data on the basis of loop models
[e] - Volume filling factor of the loop plasma observed in the SXT band
[f] - The analysis has been carried out (on the same strip as marked in the NIXT image) even if the loop is not clearly identified in the SXT image
[g] - Not a proper plasma loop filling factor.

5. Discussion

This work studies coronal loops by taking advantage of the complementary information provided by NIXT and Yohkoh/SXT, which observed the solar corona simultaneously. NIXT works in a softer and narrower spectral band, and its spatial resolution (1.2" pixel size) is four times higher than the other instrument, while Yohkoh/SXT allows direct temperature diagnostics by using different filters. In this work, for the first time, we have applied a diagnostic method (Paper I) which allows us to evaluate the plasma pressure inside loops observed with NIXT.

The analysis described above is based on the assumption that hydrostatic loop models provide a good description of loop plasma conditions, a well-established fact for most loops (e.g. Rosner et al. 1978). The presence of moderate subsonic siphon flows driven by pressure differences between the loop footpoints should not much affect our results, because the overall physical characteristics would not change much (Orlando et al. 1995). Shocking siphon flows instead should make loops appear highly asymmetric, an effect that is not observed on our selected loops. Finally although the exact values are, to some extent, subject to improvement, their orders of magnitude are unequivocal and represent a significant result.

Since the two instruments are sensitive to plasma at different coronal temperatures, NIXT mostly around 1 MK, SXT mostly higher than 2 MK, in general we do not expect an exact correspondence between the morphology of loops detected by the two instruments. In fact, although there is a good correspondence between the location of all the selected structures observed by the two telescopes, their morphology appears clearly different. A close inspection of loop structure **A** shows that the path chosen along the loop in the NIXT image corresponds to a relatively "dark" structure related to the surrounding loops in the SXT images. A more detailed analysis, which includes the pressure and filling factor evaluations in both instrument bands, seems to indicate that the two instruments are looking at distinct loop structures with different lengths, falling in the same field of view. In other words the low pressure derived from NIXT data would be confined in a loop not visible by the SXT, which, instead, detects the emission from co-existing higher pressure and more compact structures.

The pressure values obtained from SXT data are systematically higher than those obtained from NIXT. This result can probably be ascribed to the different spectral bands: the SXT is sensitive to hotter plasma, which is in general also at higher pressure for the same loop length. This indicates that plasmas at different temperature and pressure may coexist in the same loop structures, or, at most, in neighboring loops. Notice that our analysis shows that density values inferred from the emission measure as in Eq. (2) can be wrong and can lead to unrealistic values of pressure and filling factor.

The same detailed comparison cannot be made for the smaller loops **B**, **C** and **E** because of the limited resolution of the SXT. The morphology of such more compact regions appears quite similar in the SXT and NIXT images. The brightest parts detected by SXT are located close to the center of the NIXT-imaged structures and seem to coincide with the apex of the loops. For the small loops, it appears as if the combination of SXT and NIXT images would show the entire loop structure, NIXT being more sensitive to the footpoints and SXT to the apex. However, the relatively low resolution of the SXT does not allow us to put a tighter constraint on this aspect, and we cannot exclude, for instance, that the two instruments observe two adjacent loops at different pressure (SXT observing a loop at higher pressure).

We could not identify a clear counterpart of the structure **D** on the SXT images, probably because it is a relatively low pressure loop located in a region with other complex and relatively bright structures.

These results allow us to derive a more complete scenario than previously obtained, for instance, by Yoshida et al. (1995). In summary, smaller and higher pressure structure are those showing the better morphological agreement between NIXT and SXT. In contrast, large structures (**A** and **D**) appear different to the two instruments both in morphology and in plasma parameters. In particular, the large loop **A**, clearly visible in the NIXT image, is not visible in the SXT band.

The filling factor in region **A**, as observed by NIXT, is large and close to 1; for the smaller structures of regions **B**, **C** and **E**, for which a comparison between NIXT and SXT results is sound, we find a large filling factor in Yohkoh-imaged loops and a small one in NIXT-imaged ones.

All these results may be interpreted in the light of the following scenario, known since Skylab observations: coronal loops evolve from small, hot and compact structures to progressively large, cool and extended structures. Our results add the information that smaller loops are also completely filled with high temperature plasma, detectable almost only by SXT. As they get cooler, more and more plasma filaments become visible by NIXT, although coexisting with many other hot and dense filaments. Later in the cooling, most of the loop would contain relatively cooler plasma, i.e. visible with NIXT only, and with a high filling factor. The fact that this occurs just for the large loop **A** is consistent with the general trend of the gradual expansion of small loops to large loops.

In this scenario, the large loop observed by NIXT in region **A** would be a relatively evolved and cool structure, invisible to the SXT (which instead detects under/overlying hotter structures); the more compact loops in **B**, **C** and **E**, would instead be hotter and with a small number of filaments visible by NIXT; region **D** would be in an intermediate stage between the two extremes.

We note that the low filling factors obtained for the compact loops (1/100 – 1/1000) strongly suggest that there is a very fine filamentation of magnetized loops within loops and provide a quantitative estimate of its value. This work therefore contributes quantitatively to the comprehension of the filamentary structure of coronal magnetic loops. Also our findings suggest that the plasma does not cool down uniformly in the loop, and that a progressively higher number of filaments get cooler, and thus become gradually visible by NIXT. This hypothesis needs further checks and verification which will surely come from forth-coming high resolution observation.

Acknowledgements. VDM, FR and GP acknowledge partial support from Ministero dell'Università e della Ricerca Scientifica e Tecnologica, Agenzia Spaziale Italiana. LG acknowledges support from NASA grant NAGW-4081.

References

Golub L., Herant M., 1989, Proc. Spie, 1160, 629.
Golub L., Herant M., Kalata K., et al., 1990, Nature, 344, 842.
Gomez D. O., Martens P. C. H., Golub L., 1993, ApJ, 405, 767.
Litwin C., Rosner R. 1993, ApJ, 412, 375.
Orlando S., Peres G., Serio S., 1995, A&A, 294, 861.
Parker E. N., 1988 ApJ 330 474.
Peres G., Reale F., Golub L. , 1994, ApJ, 422, 412 (Paper I).
Rosner R., Tucker W., Vaiana G., 1978, ApJ, 220, 643.
Serio S., Peres G., Vaiana G.S., Golub L., Rosner R., 1981, ApJ, 243, 288.
Tsuneta S., Acton L., Bruner M., et al., 1991, Sol.Phys., 136, 37.
van den Oord G.H.J., 1992, in Solar Physics and Astrophysics at Interferometric Resolution, L. Damè & T-D. Guyenne eds., ESA SP-344, p.97
Vaiana G. S., 1976, Phil. Trans. R. Soc. Lond., A.281, 365.
Velli M., 1995, in Solar Wind 8 Conference, 28.
Yoshida T., Tsuneta S., Golub L., Strong L., Ogawara Y., 1995, P.A.S.J., 47, L15.